Available online at www.sciencedirect.com
ScienceDirect
Cement & Concrete Composites 29 (2007) 421–432
Cement & Concrete Composites
www.elsevier.com/locate/cemconcomp

Interfacial shear stress in FRP-plated RC beams under symmetric loads

Jian Yang [a], Jianqiao Ye [b,c,*], Zhongrong Niu [c]

[a] School of Engineering, University of Birmingham, Edgbaston, Birmingham B15 2TT, UK
[b] School of Civil Engineering, University of Leeds, Leeds LS2 9JT, UK
[c] School of Civil Engineering, Hefei University of Technology, Hefei 230009, PR China

Received 20 January 2006; received in revised form 27 November 2006; accepted 28 November 2006
Available online 19 January 2007

Abstract

A recently popular method for retrofitting reinforced concrete (RC) beams is to bond fibre-reinforced polymer (FRP) plates to their soffits. An important failure mode of such plated beams is debonding of the FRP plates from the concrete due to high level interfacial stresses near the plate ends. A closed-form rigorous solution for the interfacial stresses in simply supported beams bonded with thin plates and subjected to arbitrary loads has been found, in which a non-uniform stress distribution in the adhesive layer was taken into account. This paper uses the rigorous solution to investigate the impact of symmetric loading configurations on the interfacial shear stress distributions, and concludes that the bending moments on the cross sections at the plate ends play a significant role in terms of stress concentration, while the shear forces on the same cross-section contribute little to the concentration. On the basis of this observation, this paper proposes a simplified approximate solution to the shear stress along the interface between concrete and adhesive layer. Compared with the rigorous and other approximate solutions, the simplified solution exhibits sufficient accuracy in terms of stress distribution and stress concentration localized near the plate ends. Due to its compact feature, the simplified solution is more suitable for engineering applications using a portable calculator and to be adopted in the codes of practices.

Keywords: Concrete beams; FRP plates; Interfacial shear stress

1. Introduction

As a nation's infrastructure ages, one of the major challenges the construction industry faces is that the number of deficient structures continues to grow. The applications of using externally bonded steel plates or fibre reinforced polymer (FRP) laminates to reinforced concrete (RC) structures have shown that the technique is sound and efficient and offers a practical solution to this pressing problem. Retrofitting using externally bonded plates is quick, easy with respect to material handling, causes minimal site disruption and produces only little changes in section size.

Central to the reinforcement effect of externally bonded concrete structures is the transferring of stresses from the concrete to the external reinforcement, which can cause the undesirable premature and brittle failure modes, such as debonding initiated from the cut-off ends of the bonded sheets/plates [30]. A good understanding of this problem is thus important for the development of suitable strength models. Extensive studies have been carried out during the last decade to investigate the interfacial stress distributions.

A number of experimental results showing the interfacial stresses can be found in the literature, e.g. the work reported by MacDonald and Calder [17], Jones et al. [14], Garden et al. [11], Etman and Beeby [10], Ahmed et al. [1] and Maalej and Bian [16]. Bonacci and Maalej [7] compiled an experimental database from the published results, where test results from a total of 127 specimens tested in 23 separate studies were included.

Numerical methods used in the determination of the interfacial stresses include the linear finite element methods

* Corresponding author. Address: School of Civil Engineering, University of Leeds, Leeds LS2 9JT, UK. Tel.: +44 113 343 2327.
E-mail address: j.ye@leeds.ac.uk (J. Ye).

0958-9465/$ - see front matter © 2006 Elsevier Ltd. All rights reserved.
doi:10.1016/j.cemconcomp.2006.11.011

Nomenclature

A	area of the cross section transformed to bonded plate material
B	breadth of RC beam
b	breadth of bonded plate and adhesive layer
E_c	elastic modulus of concrete
$E_x^{[i]}$, $E_y^{[i]}$	elastic moduli of the ith layer in the x and y directions, respectively
f_{cu}	cube strength of concrete
$G_{xy}^{[i]}$	shear modulus of the ith layer
h_0	distance from the neutral axis to the lower edge of the cross section transformed to bonded plate material
$h^{[i]}$	thickness of the ith layer
I	second moment of area of the cross section transformed to the bonded plate material
K	coefficient in the shear stress solution for the 1st group of loading
L	half span of beam
l	half length of bonded plate
M_0	applied bending moment
M_l	bending moment on the cross sections of RC beam at plate end
q	load intensity of UDL or magnitude of point load
$q(x)$	symmetrically distributed transverse load
Q_l	shear force on the cross sections of RC beam at the plate end
S_1, S_2, S_3	parameters defined by Eqs. (A2a–c) and the simplified versions by Eq. (9)–(11)
x^*	distance away from plate end where shear stress approaches the peak value
σ_{xy}	interfacial shear stress at the AC interface in plated beam
$[\sigma_{xy}]_{max}$	maximum shear stress value
$\sigma_{xy,1}$, $\sigma_{xy,2}$	interfacial shear stress under 1st and 2nd group of loadings, respectively
σ^*	concrete fiber tensile stress at the middle span of RC beam
$v_{xy}^{[i]}$	Poisson's ratio of the ith layer
$\xi^{(1)}$	parameter defined by Eq. (A1a) and the simplified version by Eq. (4)
$\xi^{(2)}$	parameter defined by Eq. (A1b) and the simplified version by Eq. (6)
η	parameter defined by Eq. (A1c) and the simplified version by Eq. (7)
Θ	parameter defined by Eq. (A2f)
γ_1, γ_2	parameters defined by Eq. (A2d and e)

in Mays and Turnball [19], Hutchinson and Rahimi [13], Taljsten [28], Malek et al. [18], Rabinvich and Frostig [22] and Teng et al. [31]; the nonlinear finite element methods in Ziraba and Baluch [37], Ascione and Feo [6], Rahimi and Hutchinson [23] and Aprile et al. [2]; and the discrete section analyses in Arduini et al. [3], Arduini and Nanni [4], Arduini and Nanni [5] and Wang and Restrepo [33].

A number of approximate analytical solutions for calculating the interfacial stresses in simply supported FRP plated RC beams include the elastic shear stress analysis approach by Mukhopadhyaya and Swamy [20,21]; the shear-lag approach by Triantafillou and Deskovic [29], Ye [36] and Leung et al. [15]; the staged analysis approach by Roberts [24], Roberts and Haji-Kazemi [25] and the deformation compatibility-based approach by Vilnay [32], Taljsten [28], Malek et al. [18] and Smith and Teng [27]. These solutions were developed based on the assumption that shear and normal stresses are uniformly distributed across the thickness of the adhesive layer. Although this assumption reduces the complexity of the problem, leading to a relatively simple closed-form solution, it violates the traction free condition at the cut-off ends of the adhesive layer.

Rabinvich and Frostig [22] developed a high-order analysis in which the adhesive layer was treated as an elastic medium with negligible longitudinal stiffness. This leads to a uniformly distributed shear stress and a linearly distributed transverse normal stress across the thickness of the adhesive layer. The solution satisfies the traction free conditions at the ends of the adhesive layer. However, the solution does not give explicit expressions for the interfacial stresses. Shen et al. [26] proposed an alternative analytical approach which led to closed-form expressions. This analysis is limited to solve problems involving only uniformly distributed loads or/and symmetrical end moments. Yang et al. [35] extended their work to cover arbitrary loading configurations that are decomposed into symmetrical and antisymmetrical loads. However, this solution is very complex and cannot be used conveniently in the engineering practice. It is, therefore, imperative to revise the solution so that it is simple, practical and can still provide sufficient accuracy, compared with the original one.

To this end, this paper studies the general impact of symmetrically applied loads on the interfacial shear stress, and finds that the bending moments carried by the cross sections at the plate cut-off ends play a dominant role in generating stress concentration. The shear forces on the same cross sections contribute little towards the concentration, while their overall contribution to the shear stress distribution along the interface between concrete and adhesive layer can be calculated on the basis of the classic laminated beam theory.

2. Rigorous solution

As the rigorous solution of Yang et al. [35] is used to investigate the impact of load configurations to the interfa-

cial stress distribution, we adopt that model and introduce some modifications, so that it can be used for the purpose of this paper. We consider a simply supported RC beam with a span of $2L$. The bonded plate has a length of $2l$. The origin of the Cartesian coordinate system for the analysis is chosen at the top surface of the middle span (Fig. 1). In the following deductions, superscripts [1], [2] and [3] are used to denote the plate, adhesive layer and RC beam of the strengthened beam respectively. For example, $h^{[1]}$, $E_x^{[1]}$, $E_y^{[1]}$, $G_{xy}^{[1]}$ and $v_{xy}^{[1]}$ denote thickness, Young's modulus, shear modulus and Poisson's ratio of the bonded plate, respectively. B and b are the respective breadths of the concrete and the bonded plate. It is apparent that the adhesive layer and the bonded plate have the same breadth b (Fig. 2b).

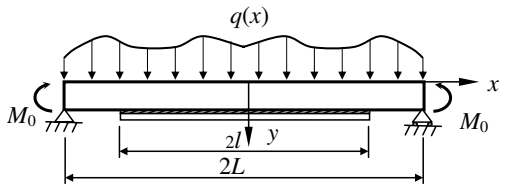

Fig. 1. A strengthened beam under symmetric loads.

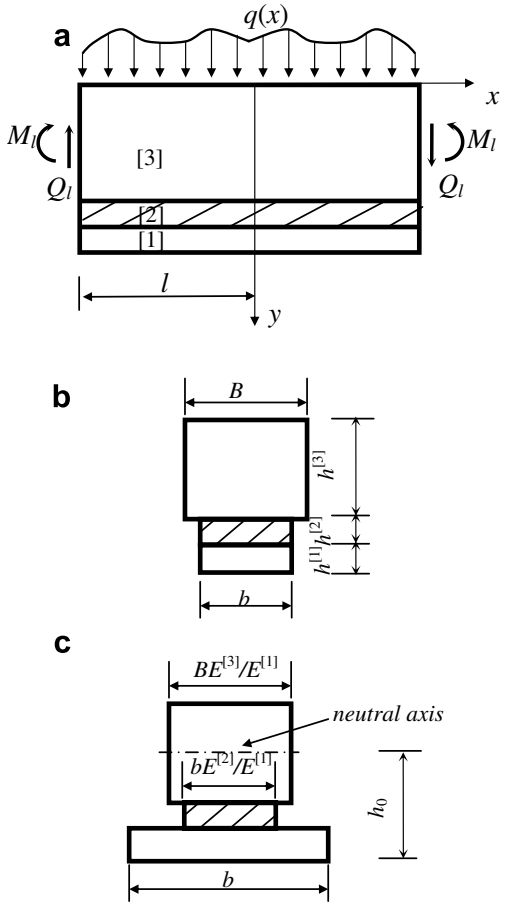

Fig. 2. Geometry and notation of a strengthened beam. (a) Configuration. (b) Cross section. (c) Equivalent cross section transferred to the plate material.

For the debonding failure mode, observations from laboratory tests have shown that a debonding crack usually initiates from the tip of the interface between the adhesive layer and concrete that is referred as AC interface in the following study. Although a substantial amount of work, e.g. those in the abovementioned references, has been done in this aspect, the exact mechanism of the debonding failure and the prediction of consequent failure load are still not clearly known. Nevertheless, it has been consistently recognized that stress concentration is the main triggering factor for this type of failure mode. Hence, the interfacial shear and normal stresses and, particularly, their distributions near the cut-off ends in the AC interface have become the center of the problem.

The stress concentration is attributed to the occurrence of material and geometrical discontinuity. In the context of linear elasticity theory it is associated with the phenomenon of stress singularity, where stress components approach infinity. There are a number of locations, e.g. in the interface of the dissimilar material and at the geometric corner, where the stress singularity may occur [34]. It has been accepted that even at a single location and after introducing the idealizations to the material properties and geometric sizes, the analysis of the stress singularity is still considerably complex, not to mention the influences of the heterogeneous materials properties and multiple cracks that the plated RC beams may show. Accordingly, in this study we adopt the same assumptions as those used in Yang et al.'s [35], which assume that all the materials are in their elastic regions and no cracks have developed in the concrete before the debonding crack is initiated. It is worth noting that there may exit flexural or shear/flexural cracks in the high bending moment zone. However, as these cracks are most likely away from the plate ends, their effects on the stresses near plate ends are ignored in this paper. Only the interfacial shear stress is computed and studied in this paper, because it is believed that there exist consistent correlations between the maximum shear stress and the corresponding debonding loads. This shear stress solution may be further exploited to develop pertinent debonding strength models.

2.1. Impact of load patterns on the interfacial shear stress in the AC interface

For a plated beam subjected to arbitrary transverse symmetrical loads, the internal forces acting on the cross sections at the cut-off ends are bending moments and shear forces. Considering the equilibrium of the strengthened part (see Fig. 2a), we separate the loads into two groups, i.e. (1) a pair of equal bending moments M_l and (2) the imposed transverse loads $q(x)$ along with the induced shear forces Q_l on the cross sections at the cut-off ends. For the transverse loads, symmetric point loads and uniformly distributed pressures are considered in this study.

Using the rigorous solution of Yang et al. [35] to investigate the impact of the load patterns on the interfacial

shear stresses, we may study the distributions of the normalized interfacial shear stresses along the AC interface with the abovementioned two groups of loadings. These are the following three cases.

2.1.1. Normalized interfacial shear stress of the plated beam subjected to bending moments

If only the strengthened part is considered, the applied loads induce a pair of bending moments M_l on the cross sections at the cut-off ends (Fig. 3). We normalize the obtained interfacial shear stress in the AC interface by σ^* and show the results in Fig. 3. Here σ^* denotes the maximum longitudinal tensile stress in the concrete obtained from the classic laminate beam theory [12], i.e. $\sigma^* = bE_x^{[3]}M_l(h_0 - h^{[1]} - h^{[2]})/BE_x^{[1]}I$, in which, h_0 is the distance from the neutral axis to the lower edge of the cross-section transferred to FRP material as defined in Eq. (A1d) and I is the second moment of the transferred cross-sectional area about its neutral axis [see Eq. (A1f)].

The distribution of the interfacial shear stress presented in the figure clearly shows that the shear stress increases exponentially starting from about $0.2l$ away from the centre and reaches its maximum at a location very close to the cut-off end. The stress then drops to zero abruptly. The maximum shear stress is about one quarter of the maximum longitudinal tensile fiber stress in concrete under the given loads. The solution is significantly different to the one from the classical laminated beam theory that provides a negligible shear stress along the interface.

2.1.2. Normalized interfacial shear stress of the strengthened beam under symmetrical point loads

Similarly, we only consider the strengthened part, which is now subjected to a pair of point loads q at $l/2$ away from the cut-off ends. Apart from the bending moments, a pair of internal shear forces $Q_l = q$ acting upwards on the cross sections are induced to equilibrate the applied loads (Fig. 4). The bending moments on the cross section are

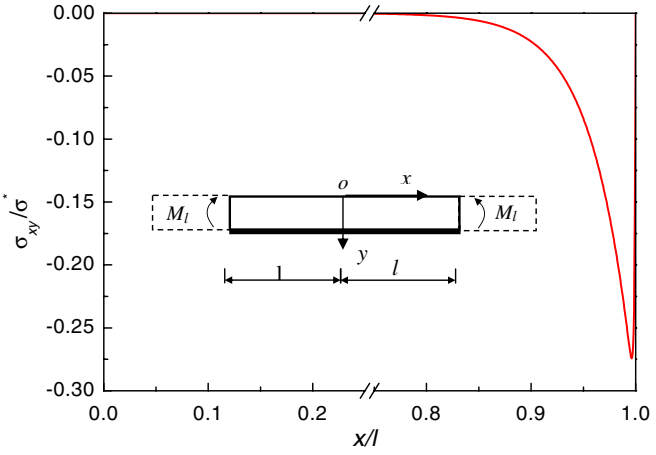

Fig. 3. Normalized shear stress along the AC interface of the strengthened beam subjected to end bending moments.

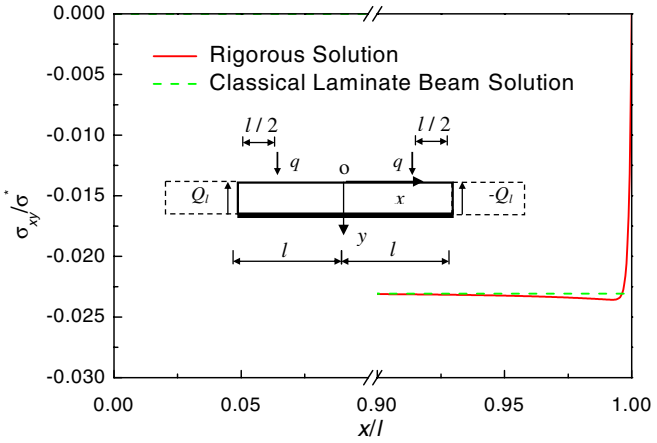

Fig. 4. Normalized shear stress along the AC interface of the strengthened beam subjected to two-point symmetric load.

omitted from Fig. 4 since its effect on the shear stress has been shown separately in Case (a). The same normalization as adopted previously is used, where the associated σ^* for the current load case is $bE_x^{[3]}ql(h_0 - h^{[1]} - h^{[2]})/2BE_x^{[1]}I$. The normalized interfacial shear stress distribution is shown in Fig. 4, along with the normalized shear stress obtained using the classic laminated beam theory.

Fig. 4 clearly shows that main difference between the two results only exists on the section near the cut-off end. The rigorous shear stress solution increases slightly when it approaches the cut-off end before dropping to zero. This gentle increase compensates the stress reduction in the vicinity of the cut-off point, such that the global equilibrium remains. The classic laminated beam solution provides a uniform shear stress distribution along the interface. The maximum interfacial shear stress is about 2.3% of the maximum tensile stress in the RC beam.

2.1.3. Normalized interfacial shear stress of the strengthened beam under a uniformly distributed load

As a different load case of the second loading group, we consider the strengthened part subjected to a uniformly

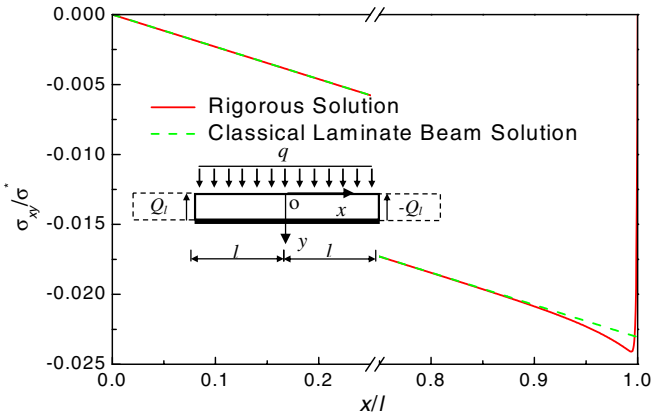

Fig. 5. Normalized shear stress along the AC interface of the strengthened beam subjected to a uniformly distributed load.

distributed load q. A pair of symmetrical shear forces $Q_l = ql$ on the cross sections at the cut-off ends are induced to maintain equilibrium (Fig. 5). The shear stress is normalized here using $\sigma^* = bE_x^{[3]}ql^2(h_0 - h^{[1]} - h^{[2]})/2BE_x^{[1]}I$. The normalized interfacial shear stress is shown in Fig. 5, where the normalized shear stress obtained using the classical laminated beam theory is also presented for comparisons.

Fig. 5 shows again that the difference between the two solutions is not significant and is only localized in the region near the cut-off end. The difference between the maximum shear stresses is only about 4%. The ratio of the maximum interfacial shear stress to the maximum tensile stress in the strengthen RC beam is identical to the one from Case (b).

2.2. Observation from the numerical examples

The above three load cases illustrate that the bending moments on the cross sections at the cut-off ends (Case (a)) dominate the interfacial shear stress concentration, while the transverse loads and the induced shear forces on the same sections (Cases (b) and (c)) have little contribution towards the concentration. Moreover, except in the vicinity of the cut-off ends, the rigorous interfacial shear stress solutions obtained for Cases (b) and (c) agree well with the solutions from the classic laminated beam theory. These observations further confirm that interfacial shear stress at any interior point in a laminated beam is predominately determined by the beam's geometry, its material properties and the internal shear force acting on the cross section at the point. This has now been well accepted and used as a principal assumption for various analyses based on the classic laminated beam theory.

Considering these observations, in the following study we will discompose any symmetric loads into two groups, i.e. (1) equal bending moments acting on the cross sections at the cut-off ends; and (2) transversely applied loads together with the shear forces induced on the same cross sections. We will simplify the rigorous interfacial shear stress solution by omitting some numerically small terms and use it for the first load group. The classic laminate beam approach will be used to obtain the interfacial shear stress for the second load group. The superposition of the solutions from these two groups provides the complete solution of the problem.

2.3. Interfacial shear stress for plated beams subjected to bending moment

In order to simplify the interfacial shear stress solution for a plated beam subjected to bending moments, we summarize the rigorous solutions obtained in Yang et al. [35] for the strengthened beam element shown in Fig. 2a. Assuming that the transverse pressure $q(x)$ and the shear force Q_l are absent, the interfacial shear stress σ_{xy} at the AC interface is

$$\sigma_{xy} = M_l \frac{3bl^3\xi^{(2)}}{BE_x^{[3]}(h^{[3]})^3\sqrt{S_2^2 - S_1}}\left(\frac{h^{[3]}\xi^{(2)}}{2} + \eta\right) \times \left[\frac{1}{l^2} - \frac{1}{l^2 + \frac{S_3}{S_1\Theta}}\right]\left[\frac{\sinh\gamma_1 x}{\sinh\gamma_1 l} - \frac{\sinh\gamma_2 x}{\sinh\gamma_2 l}\right] \quad (1)$$

where the terms are defined in Appendix A.

3. Simplified solutions

In the rigorous solutions, the terms, which are numerically small in practical engineering applications, can be omitted. For instance, Eq. (A1a) can be rearranged as

$$\xi^{(1)} = \frac{3}{h^{[1]}}\left(\frac{2 - h^{[1]}/h_0}{3 - h^{[1]}/h_0}\right) \quad (2)$$

Due to the fact that the thicknesses of both the plate and the adhesive layer are far smaller than other geometrical dimensions, i.e.

$$\mathrm{O}\left(\frac{h^{[1]}}{h_0}\right) \ll 1 \quad (3)$$

where $\mathrm{O}(x)$ denotes the order of x. Thus $h^{[1]}/h_0$ in Eq. (2) can be omitted and $\xi^{(1)}$ is then simplified as

$$\xi^{(1)} = \frac{2}{h^{[1]}} \quad (4)$$

Substituting Eq. (4) into Eq. (A1b) yields

$$\xi^{(2)} = \frac{2}{h^{[1]}}\left(1 + \frac{2E_x^{[2]}h^{[2]}}{E_x^{[1]}h^{[1]}}\right) \quad (5)$$

In practical applications, the Young's modulus of the bonded plate is far greater than that of the adhesive layer, while their thicknesses are normally comparable. It is reasonable, therefore, to ignore the second term of Eq. (5). As a result

$$\xi^{(2)} = \frac{2}{h^{[1]}} \quad (6)$$

Substituting Eqs. (5) and (6) into Eq. (A1c) leads to

$$\eta = 1 + \frac{2h^{[2]}}{h^{[1]}} + \frac{E_x^{[2]}(h^{[2]})^2}{E_x^{[1]}(h^{[1]})^2} \quad (7)$$

On the basis of the same argument as shown above Eq. (6), we may omit the last term in Eq. (7) and obtain

$$\eta = 1 + \frac{2h^{[2]}}{h^{[1]}} \quad (8)$$

Substituting the simplified coefficients of $\xi^{(1)}$, $\xi^{(2)}$ and η into Eqs. (A2a–c), respectively, yields

$$S_1 = \frac{4b}{(h^{[1]})^2}\left[\frac{4}{E_x^{[3]}h^{[3]}}\frac{b}{B} + \frac{1}{E_x^{[1]}h^{[1]}}\right] \tag{9}$$

$$S_2 = \left(\frac{2b}{h^{[1]}}\right)\left[\frac{\left(\frac{B}{b}+\frac{17b}{15B}-2\right)}{G_{xy}^{[3]}}\frac{h^{[3]}}{h^{[1]}} + \frac{1}{G_{xy}^{[2]}}\frac{h^{[2]}}{h^{[1]}} + \frac{1}{3G_{xy}^{[1]}}\right] \tag{10}$$

$$S_3 = \frac{b}{E_y^{[2]}/h^{[2]}}\left[3 + 6\frac{h^{[2]}}{h^{[1]}} + 4\frac{(h^{[2]})^2}{(h^{[1]})^2}\right] \tag{11}$$

Upon computing γ_1 and γ_2 using Eqs. (A1d) and (A1e), Eq. (1) is simplified as

$$\sigma_{xy,1} = K\left[\frac{\sinh\gamma_1 x}{\sinh\gamma_1 l} - \frac{\sinh\gamma_2 x}{\sinh\gamma_2 l}\right] \tag{12}$$

where $\sigma_{xy,1}$ denotes the interfacial shear stress generated by the first group loading, i.e., end moments. The coefficient K determines the peak value of $\sigma_{xy,1}$ along the AC interface. Representing the hyperbolic functions in Eq. (12) in the form of exponential ones, we obtain, e.g.,

$$\frac{\sinh\gamma_1 x}{\sinh\gamma_1 l} = e^{\gamma_1(l-x)}\frac{e^{2\gamma_1 x}-1}{e^{2\gamma_1 l}-1} = e^{\gamma_1(l-x)}\frac{1-e^{-2\gamma_1 x}}{e^{2\gamma_1(l-x)}-e^{-2\gamma_1 x}} \approx e^{\gamma_1(x-l)} \tag{13}$$

Thus, Eq. (12) can be further simplified as

$$\sigma_{xy,1} = K[e^{\gamma_1(x-l)} - e^{\gamma_2(x-l)}] \tag{14}$$

Eq. (14) has only one unknown coefficient K that can be determined by equating the resultant of the shear stress over the AC interface to the sum of the longitudinal tensile forces acting on the cross section at the middle span of the adhesive layer and the bonded plate. The required tensile forces can be easily computed from the classical laminated beam theory. It is also noted that $e^{-\gamma_1 l}$ and $e^{-\gamma_2 l}$ are very close to zero. Hence, the above calculation results in

$$K = \frac{M_l}{I}\frac{h_0 h^{[1]}}{\left[\frac{1}{\gamma_2}-\frac{1}{\gamma_1}\right]} \tag{15}$$

Eqs. (14) and (15) give the simplified version of the interfacial shear stress along the AC interface, which is for beams subjected to only bending moments. The interfacial shear stress approaches its peak value at $(l - x^*)$, where

$$x^* = \frac{\ln\gamma_1 - \ln\gamma_2}{\gamma_1 - \gamma_2} \tag{16}$$

The substitution of Eq. (16) into Eqs. (14) and (15) leads to

$$[\sigma_{xy,1}]_{\max} = -\frac{M_l h_0 h^{[1]}}{I}\gamma_1\left(\frac{\gamma_1}{\gamma_2}\right)^{\frac{\gamma_1}{\gamma_2-\gamma_1}} \tag{17}$$

The interfacial shear stress induced by the imposed transverse load $q(x)$ along with the corresponding shear forces is obtained using the classic laminated beam theory, as, [12]

$$\sigma_{xy,2} = -\frac{\int_0^x q(x)\,dx h_0 h^{[1]}}{I} \tag{18}$$

where the subscript 2 indicates that the solution is obtained for beams subjected to the second group loadings, and $q(x)$ is the transverse pressure acting on the top surface of the beam. For simplicity, its value at $x = l - x^*$ is computed approximately by introducing $x = l$ into Eq. (18), i.e.

$$[\sigma_{xy,2}]_{\max} = -\frac{\int_0^l q(x)\,dx h_0 h^{[1]}}{I} \tag{19}$$

Thus, the complete solution for the beam subjected to a combined action of group one and group two loadings is

$$\sigma_{xy} = \sigma_{xy,1} + \sigma_{xy,2} = \frac{h_0 h^{[1]}}{I}\left[M_l\frac{e^{\gamma_1(x-l)} - e^{\gamma_2(x-l)}}{\frac{1}{\gamma_2}-\frac{1}{\gamma_1}} - \int_0^x q(x)\,dx\right] \tag{20}$$

and the maximum shear stress is

$$[\sigma_{xy}]_{\max} = -\frac{h_0 h^{[1]}}{I}\left[M_l\gamma_1\left(\frac{\gamma_1}{\gamma_2}\right)^{\frac{\gamma_1}{\gamma_2-\gamma_1}} + \int_0^l q(x)\,dx\right] \tag{21}$$

4. Comparison with the rigorous solution

To validate the simplified expression shown in Eq. (21), the interfacial shear stresses are obtained by both the rigorous expression and its simplified form for the example beams subjected to symmetric point loads (Fig. 6) and a uniformly distributed load (Fig. 7), respectively.

In Figs. 6 and 7, the obtained shear stress distributions along the AC interface of the right half of the beam are normalized by $\sigma^* = bE_x^{[3]}q(L-l/2)(h_0 - h^{[1]} - h^{[2]})/BE_x^{[1]}I$ in Fig. 6 and $\sigma^* = bE_x^{[3]}qL^2(h_0 - h^{[1]} - h^{[2]})/2BE_x^{[1]}I$ in Fig. 7, respectively. The comparisons show encouraging agreement in both loading cases. The simplified solution is virtually identical to the rigorous solution along about 90% of the bonded length. The differences occur in the vicinity of the plate end and are most noticeable at the peak value position. The simplified solution reaches its peak value slightly farther away from the plate end and with

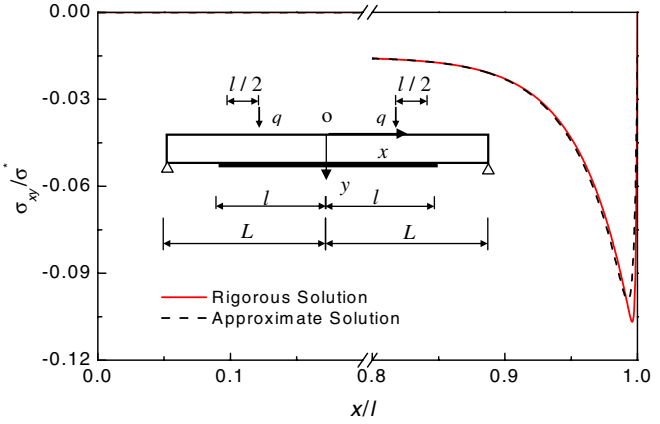

Fig. 6. Rigorous and simplified approximate solutions of the normalized shear stress along the AC interface of the strengthened beam subjected to a two-point symmetric load.

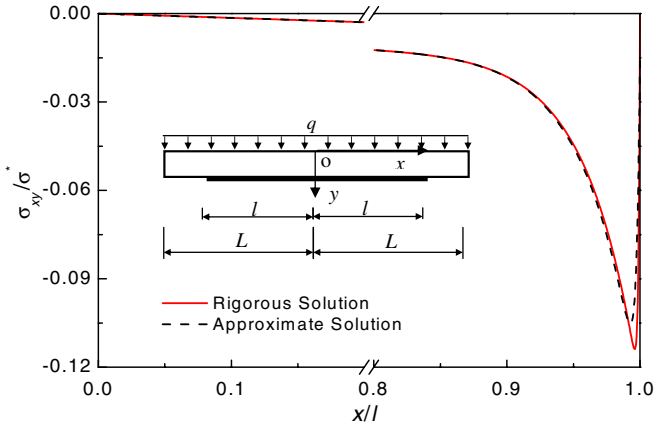

Fig. 7. Rigorous and simplified approximate solutions of the normalized shear stress along the AC interface of the strengthened beam subjected to a uniformly distributed load.

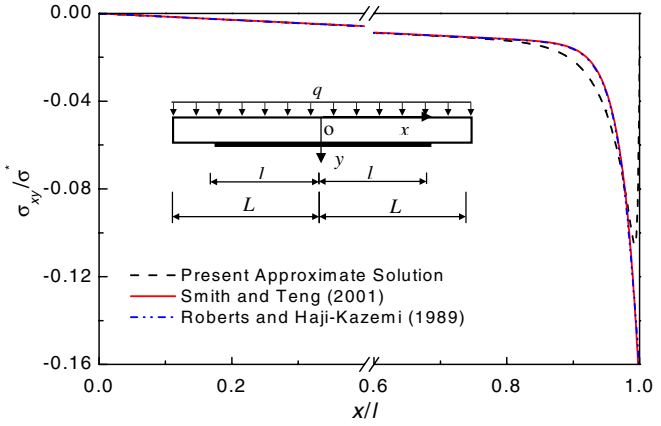

Fig. 9. Comparison of normalized shear stresses along the AC interface of the strengthened beam subjected to a uniformly distributed load.

lower value. However, as shown by the comparison, the largest relative differences of the peak values are below 10%.

5. Comparison with other approximate solutions

The present simple solution is compared, in this section, with some approximate solutions available in the literature. These include Smith and Teng's [27] and Roberts' [24] solutions for general loading and Roberts and Haji-Kazemi's [25] solution for uniformly distributed loads. All these approximate interfacial shear solutions violate the traction free condition at the cut-off ends and hence over estimate the peak shear stress.

Figs. 8 and 9, respectively, show the interfacial shear stress distribution along the interface for the beam subjected to point and uniformly distributed loads. In both cases, due to the abovementioned reason, the peak values from the present solution are about 40% lower than the approximate solutions. However, the stress resultant along the entire bonded length remain the same from different approaches, and this naturally leads to the fact that the stresses predicted by the present solution are greater than those by other approximate solution in a region of about 15% half span length immediately before the peak stress zone.

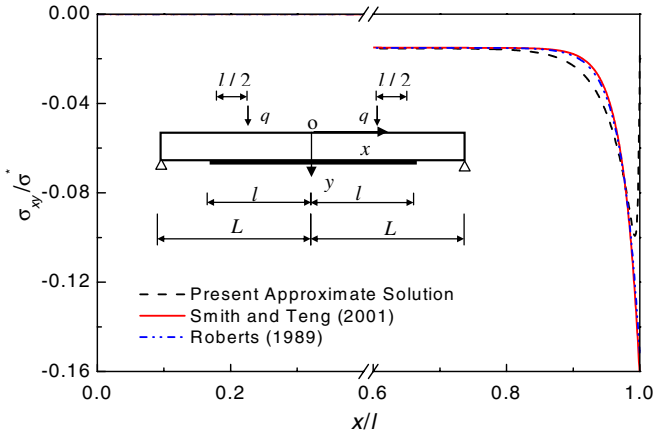

Fig. 8. Rigorous and simplified approximate solutions of the normalized shear stress along the AC interface of the strengthened beam subjected to a two-point symmetric load.

6. Comparison with experimental results

One of the tested beams bonded with steel plate by Jones et al. [14], beam F31, is analyzed here using the present simplified solution. The RC beam is simply supported and subjected to four-point bending, each at the third point. The geometrical and material properties are as follows:

$l = 1100$, $b = 125$ mm, $h^{[1]} = 6$ mm, $E^{[1]} = 200$ GPa, $v^{[1]} = 0.3$,
$h^{[2]} = 1.5$ mm, $E^{[2]} = 0.28$ GPa, $v^{[2]} = 0.3$,
$L = 1150$ mm, $B = 155$ mm, $h^{[3]} = 255$ mm, $E^{[3]} = 40$ GPa, $v^{[3]} = 0.2$.

All the above data, except the Poisson's ratio for all materials and the Young's modulus for concrete, are the original data from the test [14]. The Poisson's ratio for the adhesive material and concrete are chosen as the commonly used values. The Poisson's ratio for mild steel is taken from BS 5950-1 [8]. The Young's modulus for concrete is converted from its tested value of cube strength, which is 53.6 MPa, using $E_c = 5.5\sqrt{f_{cu}}$ in GPa [9]. All the shear moduli G are calculated using $G^{[i]} = E^{[i]}/2(1 + v^{[i]})$.

The interfacial shear stress distributions in the AC interface under the applied load 60 kN, i.e. $P = 30$ kN in Fig. 10, are compared between the experimental results and those obtained by the present method. It is noted that in the experiment the interfacial shear stress was converted from the measured plate strains at its soffit. This conversion will results in some inherent errors, such as that the stress is only the average one between strain gauges, and the measured strains also include those caused by the bending of the plate. The averaged stress apparently leads to

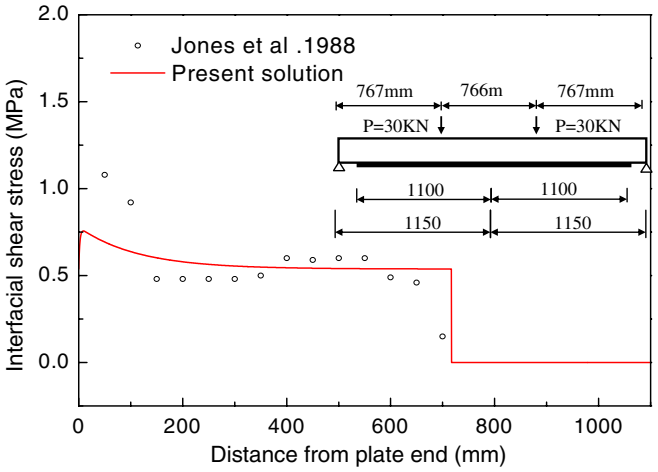

Fig. 10. Comparison of interfacial shear stress of the steel plated RC beam with the experimental results from Jones et al. [14].

underestimating of the peak stress, particularly in the region where the stress variation in the plate is severe, while the inclusion of bending stress produces a higher lever of shear stress. These generated errors may be counterbalanced, but it is not always the case. For instance, in Fig. 10, compared with the experimental results, the computed stresses near the cut-off point is underestimated because significant bending occurs in the plate therein. However, away from the plate end, they are satisfactorily close to those from the present solution.

7. Parametric studies on maximum interfacial shear stress

A strengthened beam subjected to symmetric point loads is used in this section for the parametric investigation on the effects of various parameters upon the maximum interfacial shear stress in the AC interface. The CFRP plated beam has now the following properties, unless stated otherwise:

$L = 1500$ mm, $l = 1200$ mm, $b = B = 200$ mm, $h^{[1]} = 4$ mm, $h^{[2]} = 2$ mm, $h^{[3]} = 300$ mm, $E_x^{[1]} = 100$ GPa, $E_x^{[2]} = E_y^{[2]} = 2$ GPa, $E_x^{[3]} = E_y^{[3]} = 30$ GPa, $G_{xy}^{[1]} = 5$ GPa, $v_{xy}^{[2]} = 0.35$ and $v_{xy}^{[3]} = 0.17$.

The CFRP plate is bonded symmetrically to the RC beam. The two-point loads are applied to the beam symmetrically at a distance of 1200 mm to each other and are totaled 150 kN. In the following study the peak values of the interfacial shear stress are calculated against various ratios that represent relative values of some important material and geometric parameters.

7.1. Stiffness ratio:stiffness of bonded plate to stiffness of concrete

The stiffness ratio is defined by $bE_x^{[1]}(h^{[1]})^3/BE_x^{[3]}(h^{[3]})^3$ that is a compound quantity in terms of breadths, Young's moduli and heights of the bonded plate and the RC beam. Any variation of the individual geometric or material parameters varies the ratio. To investigate the effect of the ratio, we alternate only either Young's modulus or height of the bonded plate. We consider four different Young's moduli, i.e., $E_x^{[1]} = 50$ GPa, 100 GPa, 150 GPa and 200 GPa, for each of which, $h^{[1]}$ takes 2 mm, 3 mm and 4 mm, respectively. Hence 12 maximum shear stresses are calculated for the associated stiffness ratios. Fig. 11 presents these 12 maximum shear stresses in four groups, each of which is shown by a solid line and is related to a constant Young's modulus. The three dashed lines connect the peak shear stresses for beams with a constant plate thickness but varying Young's modulus. From Fig. 11, it can be seen that both the thickness and Young's modulus have significant effects on the maximum shear stress, which is shown by the fact that an increase of their values leads to an increase of the peak shear stress. However, the combined effect, which is indicated by the relationship between the stiffness ratio and the peak stress, shows that a higher ratio may not necessarily generate a higher value of peak stress. Therefore, in a practical design, a reduction in the stiffness of bonded plate will not always reduce the possibility of the occurrence of debonding.

7.2. Thickness ratio:thickness of adhesive layer to thickness of bonded plate

Following the same procedure as used in Section 7.1, here the effects of the thickness ratio, $h^{[2]}/h^{[1]}$, on the maximum shear stress are examined. It is assumed that $h^{[1]}$ takes 2 mm, 3 mm and 4 mm, at each of which three thicknesses, i.e., 1 mm, 2 mm and 3 mm, are considered for $h^{[2]}$. Fig. 12 presents the results in six groups where stresses related to the same $h^{[1]}$ are connected by solid lines, while the dashed lines connect the results for the beams having the same values of $h^{[2]}$. It can be seen that a change of the individual thickness results in predictable changes in the stress. For instance, an increase of the plate thick-

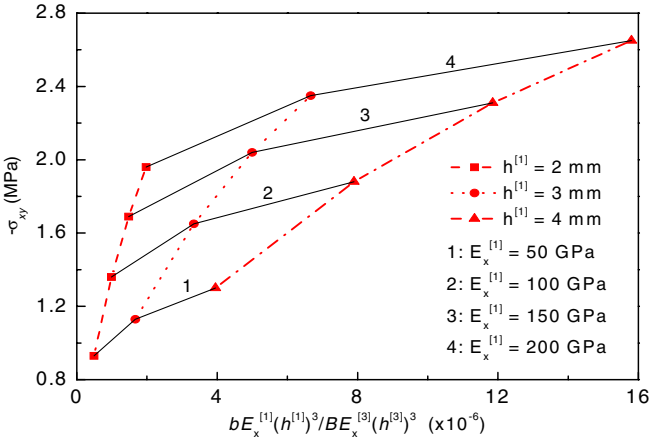

Fig. 11. Ratio of stiffness against maximum shear stress at the AC interface.

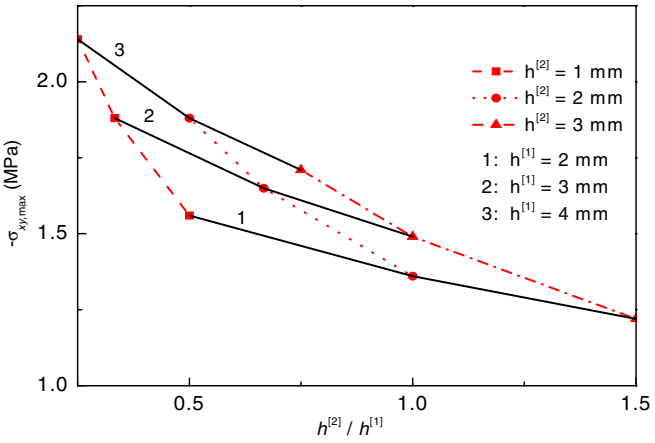

Fig. 12. Ratio of thickness against maximum shear stress at the AC interface.

ness will increase the peak value. A change of the thickness ratio, however, does not necessarily result in a desirable change in the peak stress. Hence the design of the thickness of an adhesive layer should not be entirely based on its ratio to the bonded plate.

7.3. Thickness ratio:thickness of adhesive layer to depth of concrete beam

The effect of the thickness ratio to be studied here is $h^{[2]}/h^{[3]}$. $h^{[2]}$ once again takes 1 mm, 2 mm and 3 mm and for each of the thickness, $h^{[3]}$ is set as 200 mm, 300 mm and 400 mm, respectively. Fig. 13 presents the results for the nine cases, from which similar conclusions to as made in Section 7.2 can be drawn here regarding the effect of the thickness ratio upon the peak shear stress along the AC interface.

7.4. Ratio of shear stiffness:shear stiffness of plate to shear stiffness of concrete

The ratio of shear stiffness is defined here as $bG_{xy}^{[1]}h^{[1]}/BG_{xy}^{[3]}h^{[3]}$, where the cross-sectional areas and shear moduli of both the plate and the concrete are taken into account. We vary the ratio by changing the thickness and shear modulus of the plate, which normally represents design options in practical applications. $h^{[1]}$ takes 2 mm, 3 mm and 4 mm, at each of which, $G_{xy}^{[1]}$ is chosen as 5 GPa, 10 GPa and 15 GPa mm, respectively. The computed results are shown in Fig. 14. It is seen from the figure that shear modulus of the bonded plate has virtually no effect on the peak shear stress. This is attributed to the fact that the shear stress in the bonded plate does not generate significant shear deformation with the plate due to its small thickness.

7.5. Normal constant and shear constant of the adhesive layer

The effects of the transverse normal constant $bE_y^{[2]}/h^{[2]}$ and the shear constant $bG_{xy}^{[2]}/h^{[2]}$ of the adhesive layer are studied in this section. As the adhesive layer is assumed to be isotropic, the shear modulus is proportional to the Young's modulus as $G_{xy}^{[2]} = E_x^{[2]}/2(1+v^{[2]})$ and $E_x^{[2]} = E_y^{[2]}$. Here $E_y^{[2]}$ takes 1 GPa, 2 GPa and 3 GPa, respectively, and $h^{[2]}$ 2 mm, 3 mm and 4 mm. Fig. 15 shows the effect of $bE_y^{[2]}/h^{[2]}$ on the peak values of shear stress. The figure also shows the effect of $bG_{xy}^{[2]}/h^{[2]}$, which is obtained in a straightforward manner by scaling the horizontal axis with $1/2(1+v^{[2]})$. It is evident that both constants have significant impact on the peak shear stress at the AC interface. These can be taken as amongst other dominant factors in designing thickness or stiffness of adhesive layers.

7.6. Breadth of bonded plate

To illustrate how the breadth of bonded plate affects the peak shear, we consider plates with $b = 50$ mm, 100 mm, 150 mm and 200 mm, respectively. Fig. 16 shows their effects on the peak values of interfacial shear by the present solution. It can be seen that in general a wider plate induces a higher level of shear stress for a given breadth of RC beam. When the bonded plate is very narrow, the effect

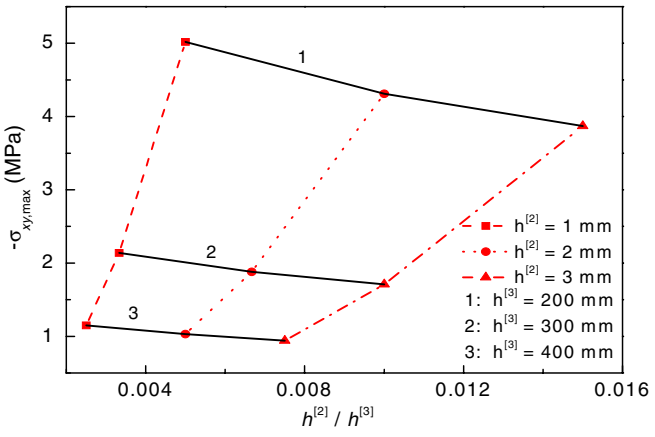

Fig. 13. Ratio of thickness against maximum shear stress at the AC interface.

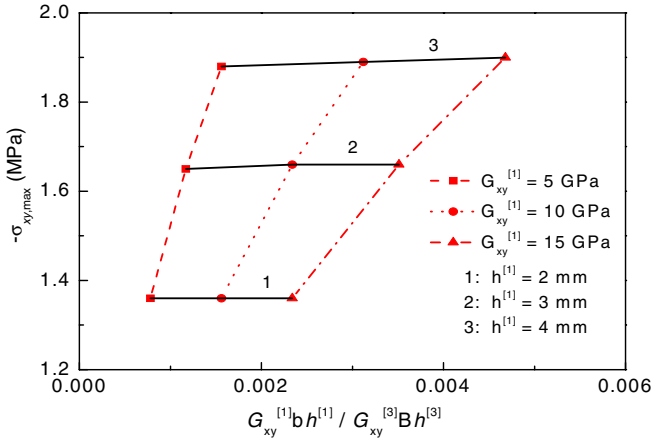

Fig. 14. Ratio of shear stiffness against maximum shear stress at the AC interface.

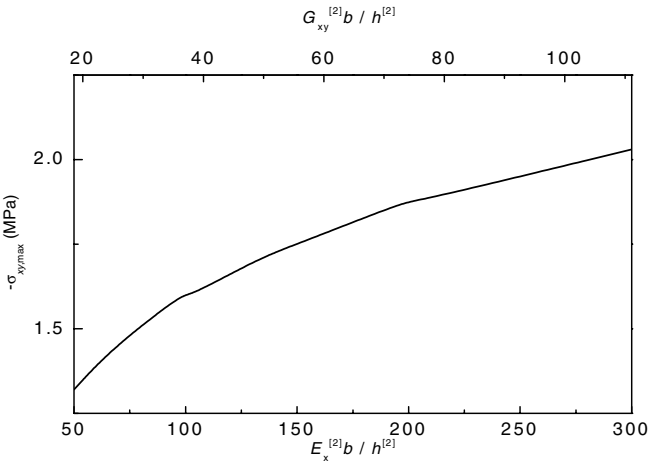

Fig. 15. The normal and shear constants of the adhesive layer against maximum shear stress at the AC interface.

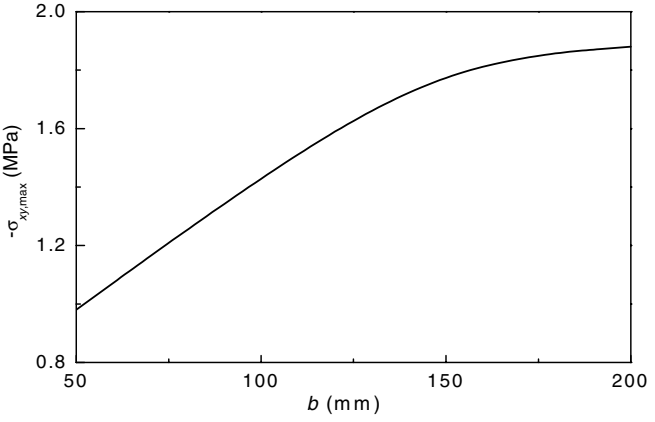

Fig. 16. Breadth of bonded plate against maximum shear stress at the AC interface.

of the breadth on the interfacial shear stress is significant, while the effect becomes less significant gradually when the breadth of the plate approaches the breadth of the beam. It is worth noting that due to the two dimensional feature of the present method, the interfacial shear stress is uniformly spread cross the plate width; hence it disregards the stress concentration due to the geometrical discontinuity in the direction of width. However, in the case of narrow plates (with less than half of the beam), this disregard of stress concentration will lead to a significant error and a 3-D method should be used in stead.

8. Conclusions

This paper investigated the impact of the internal forces on the cross sections at the cut-off ends generated by symmetrically applied loads on the shear stress along the adhesive–concrete interface of bonded RC concrete beams. Yang et al.'s [35] rigorous solutions were used in this investigation. It was found that stress concentrations occurring at the cut-off ends were mainly induced by the internal bending moments on the cross sections of the concrete beam at the cut-off ends. The internal shear forces' contributions to the interfacial shear stress were found to be very close to the solutions obtained from the classic laminated beam theory, which contributed little towards the stress concentration.

On the basis of this observation, this paper proposed a simplified approximate solution by omitting some numerically minor terms in the rigorous solution. This simplified solution eliminates the complexity of the original one and is suitable for engineering applications with the aid of a portable calculator.

By comparing with the rigorous solution, other approximate solutions and experimental results, the simplified solutions provide satisfactory predictions to the interfacial shear stress in the plated beams. In the final part of this paper, extensive parametric studies were undertaken by using the simplified solution for strengthened beams with various ratios of design parameters. Observations were made based on the numerical results concerning their possible implications to practical designs.

The simplified solution to the interfacial shear stress in the FRP-plated RC beams can be further exploited to develop a design method to predict the first debonding crack load. To this end, appropriate calibrations with adequate experimental results and field test data should be carried out using the reliability analysis. This is a part of our future work.

Appendix A

In Eq. (1), $\xi^{(1)}$, $\xi^{(2)}$, η, I, S_1, S_2, S_3, γ_1, γ_2 and Θ are defined as follows:

$$\xi^{(1)} = \frac{3(2h_0 - h^{[1]})}{h^{[1]}(3h_0 - h^{[1]})} \tag{A1a}$$

$$\xi^{(2)} = \left[1 + \frac{E_x^{[2]}h^{[2]}}{E_x^{[1]}h^{[1]}}\left(4 + \frac{3h^{[2]}}{h^{[1]}}\right)\right]\xi^{(1)} - \frac{6E_x^{[2]}h^{[2]}}{E_x^{[1]}(h^{[1]})^2}\left(1 + \frac{h^{[2]}}{h^{[1]}}\right) \tag{A1b}$$

$$\eta = 1 + \frac{h^{[2]}}{2}\left(\xi^{(1)} + \xi^{(2)}\right) + \frac{E_x^{[2]}}{E_x^{[1]}}\left(\frac{h^{[2]}}{h^{[1]}}\right)^3\left(1 - \frac{h^{[1]}}{2}\xi^{(1)}\right) \tag{A1c}$$

where h_0 is the distance from the neutral axis to the lower edge of the cross section and is as follows:

$$h_0 = \frac{\frac{b(h^{[1]})^2}{2} + \frac{bE_x^{[2]}}{E_x^{[1]}}h^{[2]}\left(h^{[1]} + \frac{h^{[2]}}{2}\right) + \frac{BE_x^{[3]}}{E_x^{[1]}}h^{[3]}\left(h^{[1]} + h^{[2]} + \frac{h^{[3]}}{2}\right)}{A} \tag{A1d}$$

in which A is the transformed cross-sectional area composed of the plate material.

$$A = bh^{[2]} + \frac{bE_x^{[2]}}{E_x^{[1]}}h^{[2]} + \frac{BE_x^{[3]}}{E_x^{[1]}}h^{[3]} \tag{A1e}$$

I is the second moment of area of the transformed cross section and is expressed as

$$I = \frac{1}{12}\left[b(h^{[1]})^3 + \frac{bE_x^{[2]}}{E_x^{[1]}}(h^{[2]})^3 + \frac{BE_x^{[3]}}{E_x^{[1]}}(h^{[3]})^3\right] + bh^{[1]}\left(\frac{h^{[1]}}{2} - h_0\right)^2 + \frac{bE_x^{[2]}}{E_x^{[1]}}h^{[2]}\left(h^{[1]} + \frac{h^{[2]}}{2} - h_0\right)^2 + \frac{BE_x^{[3]}}{E_x^{[1]}}h^{[3]}\left(h^{[1]} + h^{[2]} + \frac{h^{[3]}}{2} - h_0\right)^2 \quad \text{(A1f)}$$

and

$$S_1 = \frac{4b}{E_x^{[1]}h^{[1]}}\left[\frac{3}{(h^{[1]})^2} - \frac{3\xi^{(1)}}{h^{[1]}} + (\xi^{(1)})^2\right] + \frac{4b}{E_x^{[2]}h^{[2]}}\left[\frac{3(\eta-1)^2}{(h^{[2]})^2} - \frac{3(\xi^{(1)}+\xi^{(2)})(\eta-1)}{h^{[2]}} + (\xi^{(1)})^2 + \xi^{(1)}\xi^{(2)} + (\xi^{(2)})^2\right] + \frac{4b^2}{E_x^{[3]}h^{[3]}B}\left[\frac{3\eta^2}{(h^{[3]})^2} + \frac{3\xi^{(2)}\eta}{h^{[3]}} + (\xi^{(2)})^2\right] \quad \text{(A2a)}$$

$$S_2 = \frac{b}{G_{xy}^{[1]}h^{[1]}}\left[\frac{3}{5} - \frac{h^{[1]}\xi^{(1)}}{10} + \frac{(h^{[1]})^2(\xi^{(1)})^2}{15}\right] + \frac{b}{G_{xy}^{[2]}h^{[2]}}\left[\frac{3(\eta-1)^2}{5} - \frac{h^{[2]}(\xi^{(1)}+\xi^{(2)})(\eta-1)}{10} + \frac{(h^{[2]})^2}{15}\left[(\xi^{(1)})^2 - \frac{\xi^{(1)}\xi^{(2)}}{2} + (\xi^{(2)})^2\right]\right] + \frac{1}{G_{xy}^{[3]}h^{[3]}B}\left[\frac{b^2}{5}\left[3\eta^2 + \frac{17(h^{[3]})^2(\xi^{(2)})^2}{6} + \frac{11h^{[3]}\xi^{(2)}\eta}{2}\right] - Bbh^{[3]}\left[\left(h^{[3]}\right)^2\left(\xi^{(2)}\right)^2 + \xi^{(2)}\eta\right] + \frac{B^2(h^{[3]})^2(\xi^{(2)})^2}{2}\right] - \frac{v_{xy}^{[2]}b}{5E_x^{[2]}h^{[2]}}\left[6(\eta-1)^2 + h^{[2]}[6\xi^{(1)} + \xi^{(2)} - (\xi^{(1)} + 6\xi^{(2)})\eta] + \frac{2(h^{[2]})^2}{3}\left[(\xi^{(1)})^2 - \frac{\xi^{(1)}\xi^{(2)}}{2} + (\xi^{(2)})^2\right]\right] \quad \text{(A2b)}$$

$$S_3 = \frac{h^{[2]}b}{70E_y^{[2]}}\left[13\eta^2 + 9\eta + 13 + \frac{h^{[2]}}{3}\left[\xi^{(1)}\left(11 + \frac{13\eta}{2}\right) - \xi^{(2)}\left(\frac{13}{2} + 11\eta\right)\right] + (h^{[2]})^2\left[\frac{(\xi^{(1)})^2}{3} - \frac{\xi^{(1)}\xi^{(2)}}{2} + \frac{(\xi^{(2)})^2}{3}\right]\right] \quad \text{(A2c)}$$

and

$$\gamma_1 = \sqrt{\frac{S_2 + \sqrt{S_2^2 - 2S_1S_3}}{2S_3}}$$

$$\gamma_2 = \sqrt{\frac{S_2 - \sqrt{S_2^2 - 2S_1S_3}}{2S_3}} \quad \text{(A2d and e)}$$

$$\Theta = \frac{S_3}{2\sqrt{S_2^2 - S_1}}\left[\frac{\coth l\gamma_2}{l\gamma_2} - \frac{\coth l\gamma_1}{l\gamma_1}\right] \quad \text{(A2f)}$$

References

[1] Ahmed O, Van Gemert D, Vandewalle L. Improved model for plate-end shear of CFRP strengthened RC beams. Cement Concrete Compos 2001;23:3–19.

[2] Aprile A, Spacone E, Limkatanyu S. Role of bond in RC beams strengthened with steel and FRP plates. J Struct Eng, ASCE 2001;127(12):1445–52.

[3] Arduini M, Di-Tommaso A, Nanni A. Brittle failure in FRP plate and sheet bonded beams. ACI Struct J 1997;94(4):363–9.

[4] Arduini M, Nanni A. Behavior of precracked RC beams strengthened with carbon FRP sheets. J Compos Constr 1997;1(2):63–70.

[5] Arduini M, Nanni A. Parametric study of beams with externally bonded FRP reinforcement. ACI Struct J 1997;94(5):493–501.

[6] Ascione L, Feo L. Modeling of composite/concrete interface of RC beams strengthened with composite laminates. Composites: Part B 2000;31:535–40.

[7] Bonacci JF, Maalej M. Behavioural trends of RC beams strengthened with externally bonded FRP. J Compos Constr ASCE 2001;5(2): 102–13.

[8] BS 5950-1: 2000. Structural use of steel work in building, part 1: code of practice for design – rolled and welded sections. London: British Standards Institution; 2000.

[9] BS 8110-1: 1997. Structural use of concrete, part 1: code of practice for design and construction. London: British Standards Institution; 1997.

[10] Etman EE, Beeby AW. Experimental program and analytical study of bond stress distributions on a composite plate bonded to a reinforced concrete beam. Cement Concrete Compos 2000;22:281–91.

[11] Garden HN et al. An experimental study of the anchorage length of carbon fiber composite plates used to strengthen reinforced concrete beams. Constr Build Mater 1998;12:203–19.

[12] Gere JM, Timoshenko SP. Mechanics of materials. 4th ed. London: Stanley Thornes Ltd.; 1999.

[13] Hutchinson AR, Rahimi H. Behavior of reinforced concrete beams with externally bonded fiber reinforced plastics. In: Proceedings of the 5th international conference on structural faults and repair, University of Edinburgh, vol. 3, 1993; p. 221–8.

[14] Jones R, Swamy RN, Charif A. Plate separation and anchorage of reinforced concrete beams strengthened by epoxy-bonded steel plates. Struct Eng 1988;66(5):85–94.

[15] Leung CKY. Delamination failure in concrete beams retrofitted with a bonded plate. J Mater Civil Eng ASCE 2001;13(2):106–13.

[16] Maalej M, Bian Y. Interfacial shear stress concentration in FRP-strengthened beams. Compos Struct 2001;54:417–26.

[17] MacDonald MD, Calder AJJ. Bonded steel plating for strengthening concrete structures. Int J Adhesion Adhesives 1982;2(2):119–27.

[18] Malek AM, Saadatmanesh H, Ehsani MR. Prediction of failure load of R/C beams strengthened with FRP plate due to stress concentration at the plate end. ACI Struct J 1998;95(1):142–52.

[19] Mays GC, Turnball JD. Strengthening bridges with bonded external reinforcement. Symposium on bridges-extending the lifespan, Leamington SPA, 1992; paper 3.

[20] Mukhopadhyaya P, Swamy N. Critical review of plate anchorage stresses in premature debonding failures of plate bonded reinforced concrete beams. In: Proceedings of the 4th international symposium on fibre reinforced polymer reinforcement for reinforced concrete structures, Baltimore, 1999. ACI Publication SP-188, 199, p. 359–68.

[21] Mukhopadhyaya P, Swamy N. Interfacial shear stress: a new design criteria for plate debonding. J Compos Constr, ASCE 2001;5:35–43.

[22] Rabinvich O, Frostig Y. Closed-form high-order analysis of RC beams strengthened with FRP strips. J Compos Constr, ASCE 2000;4:65–74.

[23] Rahimi H, Hutchinson A. Concrete beams strengthened with externally bonded FRP plates. J Compos Constr, ASCE 2001;5(1): 44–56.

[24] Roberts TM. Approximate analysis of shear and normal stress concentrations in the adhesive layer of plated RC beams. Struct Eng 1989;67(12):229–33.
[25] Roberts TM, Haji-Kazemi H. Theoretical study of the behavior of reinforced concrete beams strengthened by externally bonded steel plates. Proc Inst Civil Eng Part 2 1989;87:39–55.
[26] Shen HS, Teng JG, Yang J. Interfacial stresses in beams and slabs bonded with thin plate. J Eng Mech, ASCE 2001;127:399–406.
[27] Smith ST, Teng JG. Interfacial stresses in plated beams. Eng Struct 2001;23:857–71.
[28] Täljsten B. Strengthening of beams by plate bonding. J Mater Civil Eng ASCE 1997;9(4):206–12.
[29] Triantafillou TC, Deskovic N. Innovative prestressing with FRP sheets: mechanics of short-term behavior. J Eng Mech ASCE 1991;117(7):1652–72.
[30] Teng JG, Chen JF, Smith ST, Lam L. FRP strengthened RC structures. Chichester, UK: Wiley; 2002.
[31] Teng JG, Zhang JW, Smith ST. Interfacial stress in RC beams bonded with a soffit plate: a finite element study. Constr Build Mater 2002;16(1):1–14.
[32] Vilnay O. The analysis of reinforced concrete beams strengthened by epoxy bonded steel plates. Int J Cement Compos Lightweight Concrete 1988;10(2):73–8.
[33] Wang YC, Restrepo JI. Response of RC T-beams strengthened for flexure with staggered CFRP plates. J Compos Constr 2001;5(3):188–99.
[34] Yang J. Interfacial stress analysis and strengthening prediction of plated RC beams, PhD thesis, 2005, School of Civil Engineering, The University of Leeds, UK.
[35] Yang J, Teng JG, Chen JF. Interfacial stresses in soffit-plated reinforced concrete beams. Proc Inst Civil Eng, Struct Build 2004;157:77–89.
[36] Ye JQ. Interfacial shear transfer of RC beams strengthened by bonded composite plates. Cement Concrete Compos 2001;23:411–417.
[37] Ziraba YN, Baluch MH. Computational model for reinforced concrete beams strengthened by epoxy bonded steel plates. Finite Elements Anal Des 1995;20:253–71.